Abstracta

Ano XVI - N. 03

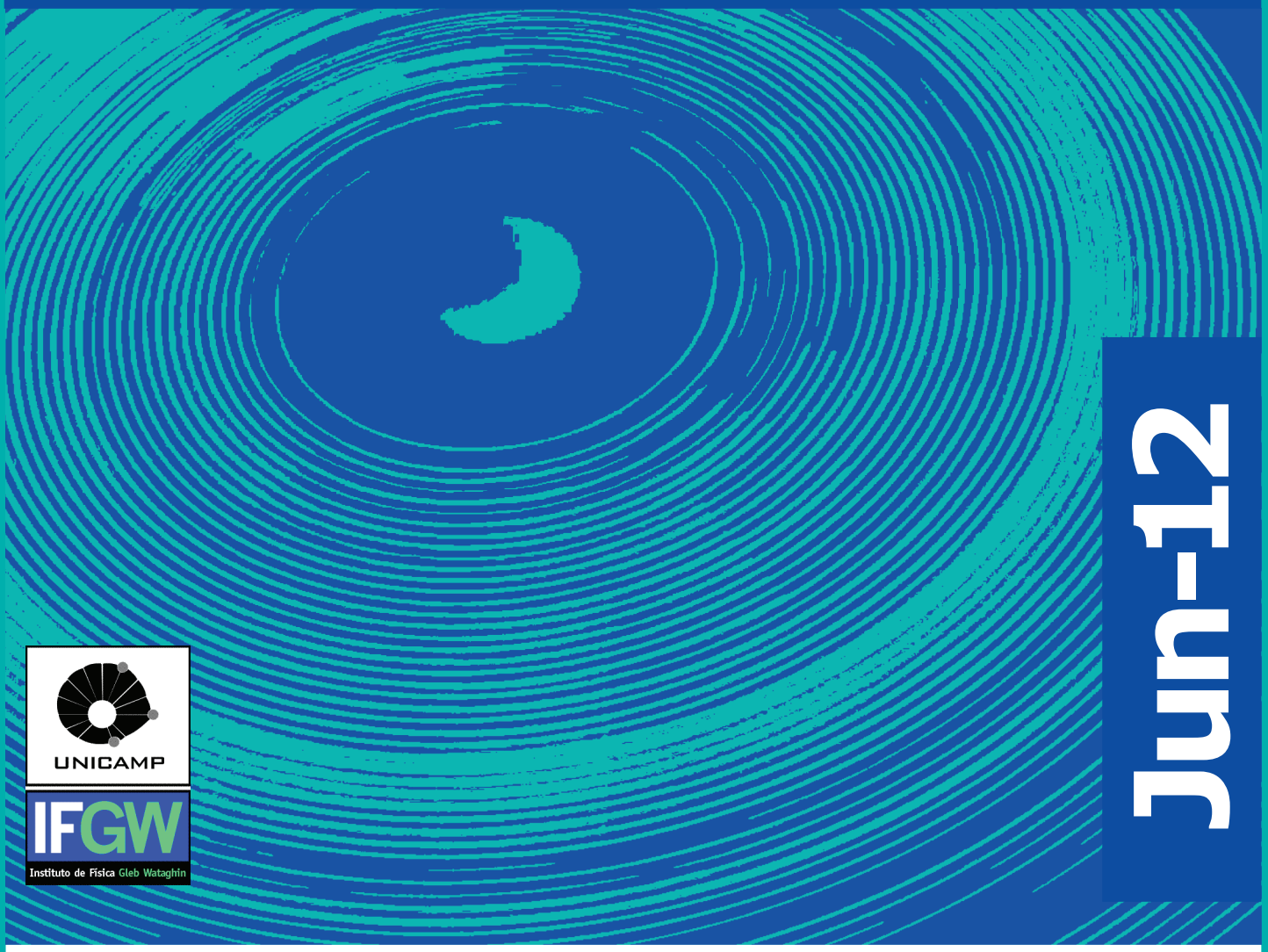

Jun-12

UNICAMP

IFGW

Instituto de Física Gleb Wataghin

Abril 2012 à Junho 2012

Trabalhos Publicados

[P076-12] "A less expensive NiMnGa based Heusler alloy for magnetic refrigeration"

Mejia, C. S.; Gomes, A. M.; de Oliveira, L. A. S.

We present a study of the substitution of Mn by Cu on the compound Ni2Mn1-xCuxGa0.9Al0.1, showing that the substitution of a small amount of Al on the Ga site does not affect the magnetic and magnetocaloric potential compared to Ni-2(Mn,Cu) Ga alloy. The samples were prepared with 10% substitution of Al and with Cu concentrations of x = 0.0, 0.2, and 0.3. Magnetization measurements as a function of temperature performed from 10 to 400 K, with an applied field of 0.02 T showed a ferromagnetic state, with critical temperature T-c = 295 and 300 K for the samples with Cu, x = 0.2 and 0.3, respectively. For the sample without Cu, a complex behavior is observed at T-c = 370 K, with martensitic transition at 220 K and a premartensitic at 250 K. Analysis of x-rays diffractograms at room temperature show a L2(1) structure for x = 0.0, while for x = 0.2 a mixture of L2(1) and martensitic is present, and the sample with x = 0.3 it is in a fully martensitic phase. Heat capacity measurements were performed in order to calculate magnetocaloric effect in the samples. The results indicate that in Ni(Mn,Cu)Ga alloys, a partial substitution of Ga by Al still produce a high refrigerant capacity while reducing the costs of fabrication.

Journal of Applied Physics 111[7], 07A923, 2012

[P077-12] "A search for anisotropy in the arrival directions of ultra high energy cosmic rays recorded at the Pierre Auger Observatory"

Abreu, P.; Aglietta, M.; Ahlers, M.; Ahn, E. J.; Albuquerque, I. F. M.; Allard, D.; Chinellato, J. A.; de Mello Junior, W. J. M.; Dobrigkeit, C.; Escobar, C. O.; Fauth, A. C.; Kemp, E.; Muller, M. A.; Selmi-Dei, D. P.; Silva, M. Z.
Pierre Auger Collaboration

Observations of cosmic rays arrival directions made with the Pierre Auger Observatory have previously provided evidence of anisotropy at the 99% CL using the correlation of ultra high energy cosmic rays (UHECRs) with objects drawn from the Veron-Cetty Veron catalog. In this paper we report on the use of three catalog independent methods to search for anisotropy. The 2pt-L, 2pt+ and 3pt methods, each giving a different measure of self-clustering in arrival directions, were tested on mock cosmic ray data sets to study the impacts of sample size and magnetic smearing on their results, accounting for both angular and energy resolutions. If the sources of UHECRs follow the same large scale structure as ordinary galaxies in the local Universe and if UHECRs are deflected no more than a few degrees, a study of mock maps suggests that these three method can efficiently respond to the resulting anisotropy with a P-value = 1.0% or smaller with data sets as few as 100 events. using data taken from January 1, 2004 to July 31, 2010 we examined the 20, 30, ... , 110 highest energy events with a corresponding minimum energy threshold of about 49.3 EeV. The minimum P-values found were 13.5% using the 2pt-L method, 1.0% using the 2pt+ method and 1.1% using the 3pt method for the highest 100 energy events. In view of the multiple (correlated) scans performed on the data set, these catalog-independent methods do not yield strong evidence of anisotropy in the highest energy cosmic rays.

Journal of Cosmology and Astroparticle Physics [4], 040, 2012

[P078-12] "Anharmonic transitions in nearly dry L-cysteine I"

Lima, T. A.; Sato, E. T.; Martins, E. T.; Homem-de-Mello, P.; Lago, A. F.; Coutinho-Neto, M. D.; Ferreira, F. F.; Giles, C.; Pires, M. O. C.; Martinho, H.

Two special dynamical transitions of universal character have recently been observed in macromolecules (lysozyme, myoglobin, bacteriorhodopsin, DNA and RNA) at T* similar to 100-150 K and T-D similar to 180-220 K. The underlying mechanisms governing these transitions have been the subject of debate. In the present work, a survey is reported on the temperature dependence of structural, vibrational and thermodynamical properties of a nearly anhydrous amino acid (orthorhombic polymorph of the amino acid L-cysteine at a hydration level of 3.5%). The temperature dependence of x-ray powder diffraction patterns, Raman spectra and specific heat revealed these two transitions at T* = 70 K and T-D = 230 K for this sample. The data were analyzed considering amino acid-amino acid, amino acid-water, water-water phonon-phonon interactions and molecular rotor activation. Our results indicated that the two referred temperatures define the triggering of very simple and particular events that govern all the interactions of the biomolecular: activation of CH2 rigid rotors (T < T*), phonon-phonon interactions between specific amino acid and water dimer vibrational modes (T* < T < T-D), and water rotational barriers surpassing (T > T-D).

Journal of Physics-Condensed Matter 24[19], 195104, 2012

[P079-12] "Anomalous optical properties of GaMnAs/AlAs quantum wells grown by molecular beam epitaxy"

Rodrigues, D. H.; Brasil, M. J. S. P.; Gobato, Y. G.; Holgado, D. P. A.; Marques, G. E.; Henini, M.

We have investigated the optical properties of GaMnAs/AlAs quantum wells (QWs) grown by molecular beam epitaxy under relatively high substrate temperatures (400 and 450 degrees C) and low Mn concentrations (<= 0.1%). We have studied the time- and polarized-resolved photoluminescence emission as a function of the laser power and an applied magnetic field. Several anomalous results have been observed including long decay times, enhancement of the diamagnetic shift and reduction in the polarization degree with increasing Mn concentration.

Journal of Physics D-Applied Physics 45[21], 215301, 2012

[P080-12] "Calculation of the centre of gravity of the cone utilizing the method of Archimedes"

Magnaghi, C. P.; Assis, A. K. T.

Archimedes calculated the centre of gravity of the cone but the proof of this theorem is not extant in his works. Knorr made a reconstruction of this proof utilizing geometrical arguments. This paper proves this theorem by means of a physical demonstration utilizing the law of the lever, and by adapting from Archimedes the method of mechanical theorems that he described in his letter to Eratosthenes.

European Journal of Physics 33[3], 637-646, 2012

[P081-12] "Catalyst Recovery and Recycling Facilitated by Magnetic Separation: Iridium and Other Metal Nanoparticles"

Jacinto, M. J.; Silva, F. P.; Kiyohara, P. K.; Landers, R.; Rossi, L. M.

The immobilization of metal nanoparticles in magnetic responsive solids allows the easy, fast, and clean separation of catalysts; however, the efficiency of this separation process depends on a strong metalsupport interaction. This interaction can be enhanced by functionalizing the support surface with amino groups.

Our catalyst support contains an inner core of magnetite that enables the magnetic separation from liquid systems and an external surface of silica suitable for further modification with organosilanes. We report herein that a magnetically recoverable amino-functionalized support captured iridium species from liquid solutions and produced a highly active hydrogenation catalyst with negligible metal leaching. An analogous Ir0 catalyst prepared with use of a nonfunctionalized support shows a higher degree of metal leaching into the liquid products. The catalytic performance in the hydrogenation of alkenes is compared with that of Rh and Pt catalysts.

Chemicatchem 4[5], 698-703, 2012

[P082-12] "Collective phase-like mode and the role of lattice distortions at T-N similar to T-C in RMn2O5 (R = Pr, Sm, Gd, Tb, Bi)"

Massa, N. E.; Garcia-Flores, A. F.; Meneses, D. D.; del Campo, L.; Echegut, P.; Fabbris, G. F. L.; Martinez-Lope, M. J.; Alonso, J. A.

We report on electronic collective excitations in RMn2O5 (R = Pr, Sm, Gd, Tb) showing condensation starting at and below similar to T-N similar to T-C similar to 40-50 K. Their origin is understood as partial delocalized e(g) electron orbitals in the Jahn-Teller distortion of the pyramid dimer with strong hybridized Mn3+-O bonds. Our local probes, Raman, infrared, and x-ray absorption, back the conclusion that there is no structural phase transition at T-N similar to T-C. Ferroelectricity is magnetically assisted by electron localization triggering lattice polarizability by unscreening. We have also found phonon hardening as the rare earth is sequentially replaced. This is understood as a consequence of lanthanide contraction. It is suggested that partially f-electron screened rare earth nuclei might be introducing a perturbation to eg electrons prone to delocalize as the superexchange interaction takes place.

Journal of Physics-Condensed Matter 24[19], 195901, 2012

[P083-12] "Comparison of Plasmonic Arrays of Holes Recorded by Interference Lithography and Focused Ion Beam"

Menezes, J. W.; Barea, L. A. M.; Chillcce, E. F.; Frateschi, N.; Cescato, L.

In this paper, we compare the geometric characteristics and the optical properties of plasmonic hole arrays recorded in gold (Au) films using two different techniques, namely, focused ion beam (FIB) and interference lithography (IL). The morphology of the samples was analyzed using a scanning electron microscope (SEM), and the plasmonic peaks were measured from the transmission spectrum of the samples. The diameters of the holes recorded by IL present approximately the same statistical deviation as those fabricated by FIB but in a much larger area. Although the transmittance measurements of both types of samples exhibit the characteristic plasmonic peaks, the intrinsic fabrication errors of each technique affect differently the optical spectra.

IEEE Photonics Journal 4[2], 544-551, 2012

[P084-12] "Delaminated vanadoaluminosilicate with [V,Al]-ITQ-18 structure"

de Pietre, M. K.; Bonk, F. A.; Rettori, C.; Garcia, F. A.; Pastore, H. O.

This paper reports on the delamination of the layered [V,Al]-Nu-6(1) to originate the [V,Al]-ITQ-18, where vanadium and aluminum were inserted in the structure by direct synthesis. The delaminated solids were obtained directly from the basic medium used for swelling, after sonication and after acid addition. Vanadium and aluminum atoms are part of the lattice sites as confirmed by Al-27-MAS-NMR,V-51-MAS-NMR and UV-Vis spectroscopy. The extent of delamination was monitored by X-ray diffraction, N-2 adsorption-desorption isotherms and Si-29-MAS-NMR. The presence of FTIR bands in the double rings region indicates that the structural unit of the initial lamellar precursor is still preserved in the delaminated materials. The material obtained after acid addition contains V5+ in extraframework octahedral and in tetrahedral sites, the first ones are easily exchanged by sodium ions. On the other hand, the material prepared only under alkaline conditions presents only framework tetrahedral V5+. The presence of the V4+ was confirmed in the lamellar precursor by EPR but the vanadium oxidation state and localization change throughout the delamination procedure.

Microporous and Mesoporous Materials 156, 244-256, 2012

[P085-12] "Description of (Pseudo-) Rapidity Density and Transverse Momentum Distributions in a Wide Energy Range (root s=22.4-7000 GeV)"

Ohsawa, A.; Shibuya, E. H.; Tamada, M.

The rapidity density and transverse momentum distributions of produced particles in multiple particle production are formulated assuming that the produced particles are emitted isotropically from several emitting centers. The energy distribution of produced particles in the rest frames of respective emitting centers is that of the Tsallis statistics. The distribution of emitting centers is flat with slanting cuts at both shoulders on the rapidity axis in the center of mass system. The formulation includes six adjustable parameters, among which four are energy dependent and more important and are determined so that the transverse momentum and the (pseudo-) rapidity density distributions fit to the data at various energies. The energy dependences of the four parameters, determined empirically, reproduce quite well the energy dependence of the average transverse momentum, that of the pseudo- rapidity density at eta* = 0 and that of the charged multiplicity. The energy dependence of the inelasticity is either increasing or decreasing from the assumed value of K = 0.5 at root s = 10 GeV, due to lack of experimental data at the most-forward rapidity region. The pseudo-rapidity density distribution at LHC energy (root s = 14 TeV) expected by the present formulation is compared with those by the other models.

International Journal of Modern Physics A 27[9], 1250043, 2012

[P086-12] "Description of atmospheric conditions at the Pierre Auger Observatory using the Global Data Assimilation System (GDAS)"

Abreu, P.; Aglietta, M.; Ahlers, M.; Ahn, E. J.; Albuquerque, I. F. M.; Allard, D.; Chinellato, J. A.; Daniel, B.; de Mello Junior, W. J. M.; Dobrigkeit, C.; Escobar, C. O.; Fauth, A. C.; Kemp, E.; Muller, M. A.; Selmi-Dei, D. P.; Silva, M. Z. Pierre Auger Collaboration

Atmospheric conditions at the site of a cosmic ray observatory must be known for reconstructing observed extensive air showers. The Global Data Assimilation System (GDAS) is a global atmospheric model predicated on meteorological measurements and numerical weather predictions. GDAS provides altitude-dependent profiles of the main state variables of the atmosphere like temperature, pressure, and humidity.

The original data and their application to the air shower reconstruction of the Pierre Auger Observatory are described. By comparisons with radiosonde and weather station measurements obtained on-site in Malargue and averaged monthly models, the utility of the GDAS data is shown.

Astroparticle Physics 35[9], 591-607, 2012

[P087-12] "Directed Flow of Identified Particles in Au plus Au Collisions at root S-NN=200 GeV at RHIC"

Adamczyk, L.; Agakishiev, G.; Aggarwal, M. M.; de Souza, R. D.; Takahashi, J. ; Vasconcelos, G. M. S. STAR Collaboration

STAR's measurements of directed flow (v(1)) around midrapidity for pi(+/-), K-+/-, K-S(0), p, and (p) over bar in Au + Au collisions at root s(NN) = 200 GeV are presented. A negative v(1) (y) slope is observed for most of produced particles (pi(+/-), K-+/-, K-S(0), p, and (p) over bar). In 5%-30% central collisions, a sizable difference is present between the v(1)(y) slope of protons and antiprotons, with the former being consistent with zero within errors. The v(1) excitation function is presented. Comparisons to model calculations (RQMD, UrQMD, AMPT, QGSM with parton recombination, and a hydrodynamics model with a tilted source) are made. For those models which have calculations of v(1) for both pions and protons, none of them can describe v(1()y) forpions and protons simultaneously. The hydrodynamics model with a tilted source as currently implemented cannot explain the centrality dependence of the difference between the v(1)(y) slopes of protons and antiprotons.

Physical Review Letters 108[20], 202301, 2012

[P088-12] "Effect of light impurities on the electronic structure of copper nanowires"

Amorim, E. P. M.; da Silva, E. Z.

Recently an interesting mechanochemical effect was found showing a possibility to produce longer copper atomic chains in nitrogen atmospheres [Amorim and da Silva, Phys. Rev. B 82, 153403 (2010)]. This work presents a systematic and comparative study of the effect of doping with H, B, C, N, O, S, and N-2 impurities to the electronic structure of copper nanowires. It was performed by means of ab initio total energy calculations based on density functional theory, using local density and generalized gradient approximations. All impurities show a sd(z)(2) bond, boron makes a sigma pd(yz) bond, while carbon, oxygen, and sulfur have a strong sigma pd(z)(2) and pi pd(yz) bond. These impurities modify the metallic chain structure of the nanowire and change chain distances in the way that can be observed in electron microscopy experiments. Nitrogen and N-2 also have a strong Phi pd(z)(2) and make a pi pd(xz) bond that is stronger than the other impurities enhancing the size of atomic chains. Small spin anisotropy is introduced through carbon, oxygen, nitrogen, and sulfur doping. Remarks about the electronic states around the Fermi level are presented.

Physical Review B 85[15], 155407, 2012

[P089-12] "Effects of Etching on Zircon Grains and Its Implications for the Fission Track Method"

Saenz, C. A. T.; Curvo, E. A. C.; Dias, A. N. C.; Soares, C. J.; Constantino, C. J. L.; Alencar, I.; Guedes, S.; Palissari, R.; Neto, J. C. H.

Studies of zircon grains using optical microscopy, micro-Raman spectroscopy, and scanning electron microscopy (SEM) have been carried out to characterize the surface of natural zircon as a function of etching time. According to the surface characteristics observed using an optical microscope after etching, the zircon grains were classified as: (i) homogeneous; (ii) anomalous, and (iii) hybrid. Micro-Raman results showed that, as etching time increases, the crystal lattice is slightly altered for homogeneous grains, it is completely damaged for anomalous grains, and it is altered in some areas for hybrid grains. The SEM (energy dispersive X-ray spectroscopy, EDS) results indicated that, independent of the grain types, where the crystallinity remains after etching, the chemical composition of zircon is approximately 33% SiO2:65% ZrO2 (standard natural zircon), and for areas where the grain does not have a crystalline structure, there are variations of ZrO2 and, mainly, SiO2. In addition, it is possible to observe a uniform surface density of fission tracks in grain areas where the determined crystal lattice and chemical composition are those of zircon. Regarding hybrid grains, we discuss whether the areas slightly altered by the chemical etching can be analyzed by the fission track method (FM) or not. Results of zircon fission track and U-Ph dating show that hybrid and homogeneous grains can be used for dating, and not only homogeneous grains. More than 50 sedimentary samples from the Bauru Basin (southeast Brazil) were analyzed and show that only a small amount of grains are homogeneous (10%), questioning the validity of the rest of the grains for thermo-chronological evolution studies using zircon FTM dating.

Applied Spectroscopy 66[5], 545-551, 2012

[P090-12] "Electron scattering by methanol and ethanol: A joint theoretical-experimental investigation"

Lee, M. T.; de Souza, G. L. C.; Machado, L. E.; Brescansin, L. M.; dos Santos, A. S.; Lucchese, R. R.; Sugohara, R. T.; Homem, M. G. P.; Sanches, I. P.; Iga, I.

We present a joint theoretical-experimental study on electron scattering by methanol (CH3OH) and ethanol (C2H5OH) in a wide energy range. Experimental differential, integral and momentum-transfer cross sections for elastic electron scattering by ethanol are reported in the 100-1000 eV energy range. The experimental angular distributions of the energy-selected electrons are measured and converted to absolute cross sections using the relative flow technique. Moreover, elastic, total, and total absorption cross sections for both alcohols are calculated in the 1-500 eV energy range. A complex optical potential is used to represent the dynamics of the electron-alcohol interaction, whereas the scattering equations are solved iteratively using the Pade's approximant technique. Our calculated data agree well with those obtained using the Schwinger multichannel method at energies up to 20 eV. Discrepancies at high energies indicate the importance of absorption effects, included in our calculations. In general, the comparison between our theoretical and experimental results, as well as with other experimental data available in the literature, also show good agreement. Nevertheless, the discrepancy between the theoretical and experimental total cross sections at low incident energies suggests that the experimental cross sections measured using the transmission technique for polar targets should be reviewed.

Journal of Chemical Physics 136[11], 114311, 2012

[P091-12] "Energy transfer dynamics and thermalization of two oscillators interacting via chaos"

Marchiori, M. A.; Fariello, R.; de Aguiar, M. A. M.

We consider the classical dynamics of two particles moving in harmonic potential wells and interacting with the same external environment H-E, consisting of N noninteracting chaotic systems. The parameters are set so that when either particle is separately placed in contact with the environment, a dissipative behavior is observed. When both particles are simultaneously in contact with H-E an indirect coupling between them is observed only if the particles are in near-resonance. We study the equilibrium properties of the system considering ensemble averages for the case N = 1 and single trajectory dynamics for N large. In both cases, the particles and the environment reach an equilibrium configuration at long times, but only for large N can a temperature be assigned to the system.

Physical Review E 85[4], 041119, Part 1, 2012

[P092-12] "Experimental and Monte Carlo-simulated spectra of standard mammography-quality beams"

David, M. G.; Pires, E. J.; Bernal, M. A.; Peixoto, J. G.; Dealmeida, C. E.

A spectrometric study of standard mammography-quality beams by using experimental and Monte Carlo simulation methods was carried out in this work. The qualities of these beams are described according to the International Electrotechical Commission 61267 standard and the Technical Report Series 457 International Atomic Energy Agency report. Specifically, the non-attenuated RQR-M beam series was studied. Methods: A Si-PIN diode-based spectrometer and the PENELOPE Monte Carlo code (v. 2008F1) were used for experiments and simulations, respectively. In addition, an ionization chamber was used to determine the half-value layers (HVLs) of each beam quality. The measurements were done in the mammography dosimeter calibration setup of our laboratory, and the Monte Carlo simulations reproduced such conditions. Results: The relative differences between the HVLs calculated from experimental and simulated spectra were lower than 2.4% for all the beam qualities studied. These differences are 1.2% and 3.1% when comparing the HVLs calculated from the experimental and simulated spectra to those determined by using the ionization chamber, respectively. A semi-empirical relation was found to obtain the nominal tube potential from the effective tube potential. Conclusion: According to our results, the mammography beams used in this work have energy spectra similar to clinical beams.

British Journal of Radiology 85[1013], 629-635, 2012

[P093-12] "Hopping Magnetotransport via Nonzero Orbital Momentum States and Organic Magnetoresistance"

Alexandrov, A. S.; Dediu, V. A.; Kabanov, V. V.

In hopping magnetoresistance of doped insulators, an applied magnetic field shrinks the electron (hole) s-wave function of a donor or an acceptor and this reduces the overlap between hopping sites resulting in the positive magnetoresistance quadratic in a weak magnetic field, B. We extend the theory of hopping magnetoresistance to states with nonzero orbital momenta. Different from s states, a weak magnetic field expands the electron (hole) wave functions with positive magnetic quantum numbers, m > 0, and shrinks the states with negative m in a wide region outside the point defect. This together with a magnetic-field dependence of injection/ionization rates results in a negative weak-field magnetoresistance, which is linear in B when the orbital degeneracy is lifted. The theory provides a possible explanation of a large low-field magnetoresistance in disordered pi-conjugated organic materials.

Physical Review Letters 108[18], 186601, 2012

[P094-12] "Improved Measurement of Muon Antineutrino Disappearance in MINOS"

Adamson, P.; Ayres, D. S.; Backhouse, C.; Coelho, J. A. B.; Escobar, C. O. MINOS Collaboration

We report an improved measurement of (nu) over bar (mu) disappearance over a distance of 735 km using the MINOS detectors and the Fermilab Main Injector neutrino beam in a (nu) over bar (mu)-enhanced configuration. From a total exposure of 2.95 x 10(20) protons on target, of which 42% have not been previously analyzed, we make the most precise measurement of Delta(m) over bar (2) = [2.62(-0.28)(+0.31)(stat) +/- 0.09(syst)] x 10(-3) eV(2) and constrain the (nu) over bar (mu) mixing angle sin(2)(2 (theta) over bar) > 0.75 (90% C.L.). These values are in agreement with Delta m(2) and sin(2)(2 theta) measured for nu(mu), removing the tension reported in [P. Adamson et al. (MINOS), Phys. Rev. Lett. 107, 021801 (2011).].

Physical Review Letters 108[19], 191801, 2012

[P095-12] "Light vector meson production in pp collisions at root s=7 TeV ALICE Collaboration"

Abelev, B.; Quintana, A. A.; Adamova, D.; Adare, A. M.; Aggarwal, M. M.; Chinellato, D. D.; Cosentino, M. R.; Dash, A.; Takahashi, J.

ALICE Collaboration

The ALICE experiment has measured low-mass dimuon production in pp collisions at root s = 7 TeV in the dimuon rapidity region 2.5 < y < 4. The observed dimuon mass spectrum is described as a superposition of resonance decays (eta, rho, omega, eta', phi) into muons and semi-leptonic decays of charmed mesons. The measured production cross sections for omega and phi are sigma(omega)(1 < p(t) < 5 GeV/c. 2.5 < y < 4) = 5.28 +/- 0.54(stat) +/- 0.49(syst) mb and sigma(phi)(1 < p(t) < 5 GeV/c. 2.5 < y < 4) = 0.940 +/- 0.084(stat) +/- 0.076(syst) mb. The differential cross sections d(2)sigma/dy dp(t) are extracted as a function of p(t) for omega and phi. The ratio between the rho and omega cross section is obtained. Results for the phi are compared with other measurements at the same energy and with predictions by models.

Physics Letters B 710[4-5], 557-568, 2012

[P096-12] "Magnetism, magnetoresistance, and Shubnikov-de Haas oscillations in Na-implanted highly oriented pyrolitic graphite"

Pires, R. F.; Pureur, P.; Behar, M.; Pimentel, J. L.; Schaf, J.; Kopelevich, Y.

We report on magnetization, magnetoresistance, and Shubnikov-de Haas oscillations experiments in Na-implanted samples of highly oriented pyrolitic graphite (HOPG). Different ion fluences were applied so that samples with Na contents of 0.5, 1.0, 1.5, and 2.0 at. % were obtained in the implanted region. Ferromagnetic-like hysteresis was observed in magnetization experiments where the field was applied parallel to the graphene planes. The observed saturation moment increases systematically as a function of the implanted ion concentration up to Na 1 at. %, where it goes through a maximum before decreasing slightly towards Na 2 at. %. The planar magnetoresistance amplitude at fixed field and temperature closely correlates with the saturation magnetization data. This result suggests that the strong planar magnetoresistance in graphite is at least partially related to a spin dependent mechanism. The magnetoresistance experiments also reveal the occurrence of Shubnikov-de Haas oscillations. The characteristic frequencies and the effective masses could be estimated and do not depend on the Na concentration.

The reported experiments show that the expressive enhancement observed in ferromagnetic-like response in Na-implanted HOPG is primarily due to point defects produced by the implantation process.

Journal of Applied Physics 111[9], 093922, 2012

[P097-12] "Measurement of event background fluctuations for charged particle jet reconstruction in Pb-Pb collisions at root s(NN)=2.76 TeV"

Abelev, B.; Adam, J.; Adamova, D.; Adare, A. M.; Aggarwal, M. M.; Chinellato, D. D.; Cosentino, M. R.; Dash, A.; Takahashi, J.

ALICE Collaboration

The effect of event background fluctuations on charged particle jet reconstruction in Pb-Pb collisions at root s(NN) = 2.76 TeV has been measured with the ALICE experiment. The main sources of non-statistical fluctuations are characterized based purely on experimental data with an unbiased method, as well as by using single high p(t) particles and simulated jets embedded into real Pb-Pb events and reconstructed with the anti-k(t) jet finder. The influence of a low transverse momentum cut-off on particles used in the jet reconstruction is quantified by varying the minimum track p(t) between 0.15 GeV/c and 2 GeV/c. For embedded jets reconstructed from charged particles with p(t) > 0.15 GeV/c, the uncertainty in the reconstructed jet transverse momentum due to the heavy-ion background is measured to be 11.3 GeV/c (standard deviation) for the 10% most central Pb-Pb collisions, slightly larger than the value of 11.0 GeV/c measured using the unbiased method. For a higher particle transverse momentum threshold of 2 GeV/c, which will generate a stronger bias towards hard fragmentation in the jet finding process, the standard deviation of the fluctuations in the reconstructed jet transverse momentum is reduced to 4.8-5.0 GeV/c for the 10% most central events. A non-Gaussian tail of the momentum uncertainty is observed and its impact on the reconstructed jet spectrum is evaluated for varying particle momentum thresholds, by folding the measured fluctuations with steeply falling spectra.

Journal of High Energy Physics [3], 053, 2012

[P098-12] "Optical Tweezers as a New Biomedical Tool to Measure Zeta Potential of Stored Red Blood Cells"

Silva, D. C. N.; Jovino, C. N.; Silva, C. A. L.; Fernandes, H. P.; Filho, M. M.; Lucena, S. C.; Costa, A. M. D. N.; Cesar, C. L.; Barjas-Castro, M. L.; Santos, B. S.; Fontes, A.

During storage, red blood cells (RBCs) for transfusion purposes suffer progressive deterioration. Sialylated glycoproteins of the RBC membrane are responsible for a negatively charged surface which creates a repulsive electrical zeta potential. These charges help prevent the interaction between RBCs and other cells, and especially among each RBCs. Reports in the literature have stated that RBCs sialylated glycoproteins can be sensitive to enzymes released by leukocyte degranulation. Thus, the aim of this study was, by using an optical tweezers as a biomedical tool, to measure the zeta potential in standard RBCs units and in leukocyte reduced RBC units (collected in CPD-SAGM) during storage. Optical tweezers is a sensitive tool that uses light for measuring cell biophysical properties which are important for clinical and research purposes. This is the first study to analyze RBCs membrane charges during storage. In addition, we herein also measured the elasticity of RBCs also collected in CPD-SAGM. In conclusion, the zeta potential decreased 42% and cells were 134% less deformable at the end of storage. The zeta potential from leukodepleted units had a similar profile when compared to units stored without leukoreduction, indicating that leukocytelyses were not responsible for the zeta potential decay. Flow cytometry measurements of reactive oxygen species suggested that this decay is due to membrane oxidative damages. These results show that measurements of zeta potentials provide new insights about RBCs storage lesion for transfusion purposes.

Plos One 7[2], e31778, 2012

[P099-12] "Patch exploitation strategies of parasitoids: The role of sex ratio and forager's interference in structuring metapopulations"

Reigada, C.; Araujo, S. B. L.; de Aguiar, M. A. M.

We use a mathematical model to explore the effects of parasitoid reproductive strategies and foraging behavior in response to spatio-temporal variations in the patch quality of a host-parasitoid metapopulation system. The variations of patch quality over the landscape were measured by the presence of parasitoid competitors and the density of hosts. The parasitoid responses to patch quality are given by three different foraging behaviors: (i) the decision to remain in or leave the current patch; (ii) the control of progeny's sex ratio and (iii) competitive abilities, measured by changes in the potential to attack hosts due to interference from conspecifics in the exploited patch. We study the dynamics of host and parasitoid populations characterized by different levels of density-dependent sex ratio adjustment and interference competition. Our results show that population stability increases when parasitoid growth is correlated with patch conditions. The effect of sex ratio adjustment alone does not account for qualitative changes to system dynamics or to the distribution patterns of species. In contrast, the degree of competitive interference among the parasitoids plays a crucial role in constraining the parasitoids' potential to reduce host populations and in determining the species' distribution in the landscape. We found that high levels of interference competition disrupt the population dynamics within a patch and allows hosts to completely dominate the landscape. This study shows that the inclusion of life history traits and the co-evolutionary aspects of host-parasitoid interaction can help researchers to understand species distribution patterns in the landscape.

Ecological Modelling 230, 11-21, 2012

[P100-12] "Positron scattering from the cyclic ethers oxirane, 1,4-dioxane, and tetrahydropyran"

Zecca, A.; Trainotti, E.; Chiari, L.; Bettega, M. H. F.; Sanchez, S. D.; Varella, M. T. D.; Lima, M. A. P.; Brunger, M. J.

In this paper we report original measurements of total cross sections (TCSs) for positron scattering from the cyclic ethers oxirane (C2H4O), 1,4-dioxane (C4H8O2), and tetrahydropyran (C5H10O). The present experiments focus on the low energy range from similar to 0.2 to 50 eV, with an energy resolution smaller than 300 meV. This study concludes our systematic investigation into TCSs for a class of organic compounds that can be thought of as sub-units or moieties to the nucleotides in living matter, and which as a consequence have become topical for scientists seeking to simulate particle tracks in matter. Note that as TCSs specify the mean free path between collisions in such simulations, they have enjoyed something of a recent renaissance in interest because of that application. For oxirane, we also report original Schwinger multichannel elastic integral cross section (ICS) calculations at the static and static plus polarisation levels, and with and without Born-closure that attempts to account for the permanent dipole moment of C2H4O. Those elastic ICSs are computed for the energy range 0.5-10 eV. To the best of our knowledge, there are no other experimental results or theoretical calculations against which we can compare the present positron TCSs.

However, electron TCSs for oxirane (also known as ethylene oxide) and tetrahydropyran do currently exist in the literature and a comparison to them for each species will be presented.

Journal of Chemical Physics 136[12], 124305, 2012

[P101-12] "Spin-Electron-Phonon Excitation in Re-based Half-Metallic Double Perovskites"

Garcia-Flores, A. F.; Moreira, A. F. L.; Kaneko, U. F.; Ardito, F. M.; Terashita, H.; Orlando, M. T. D.; Gopalakrishnan, J.; Ramesha, K.; Granado, E.

A remarkable hardening (similar to 30 cm(-1)) of the normal mode of vibration associated with the symmetric stretching of the oxygen octahedra for the Ba2FeReO6 and Sr2CrReO6 double perovskites is observed below the corresponding magnetic ordering temperatures. The very large magnitude of this effect and its absence for the antisymmetric stretching mode provide evidence against a conventional spin-phonon coupling mechanism. Our observations are consistent with a collective excitation formed by the combination of the vibrational mode with oscillations of Fe or Cr 3d and Re 5d occupations and spin magnitudes.

Physical Review Letters 108[17], 177202, 2012

[P102-12] "Stabilized photorefractive running holograms, with arbitrarily selected phase shift, for material characterization"

de Oliveira, I.; Freschi, A. A.; Fier, I.; Frejlich, J.

We report on the recording of stabilized running holograms in photorefractive materials with arbitrarily selected phase shift phi between the transmitted and difracted beams propagating along the same direction behind the photorefractive crystal. The dependence of the diffraction efficiency and of the hologram speed on phi, in such stabilized holograms, can be easily measured and used for material characterization. In this communication we applied for the first time this technique for studying and characterizing hole-electron competition in a nominally undoped titanosillenite crystal sample.

Optical Materials Express 2[3], 228-234, 2012

[P103-12] "Structural and Magnetic Studies of Co0.6Zn0.4Fe2O4 Nanoferrite Synthesized by Solution Combustion Method"

Rani, R.; Dhiman, P.; Sharma, S. K.; Singh, M.

Co0.6Zn0.4Fe2O4 nanomagnetic system is prepared by solution combustion method. The powder sample is characterized by Xray diffraction (XRD), transmission electron microscope analysis (TEM), Fourier transform infrared spectroscopy (FTIR), Mossbauer spectroscopy, and superconducting quantum interference device (SQUID; at low and room temperatures). The average crystallite sizes of the prepared samples obtained from XRD is 22 nm, which is well confirmed by the size obtained from TEM. The magnetic study shows that sample is ferromagnetic at room temperature. This result is also supported by Mossbauer spectrum obtained at room temperature.

Synthesis and Reactivity in Inorganic Metal-Organic and Nano-Metal Chemistry 42[3], 360-363, 2012

[P104-12] "Structural, optical and electrical properties of indium nitride polycrystalline films"

da Silva, M. V. S.; David, D. G. F.; Pepe, I.; da Silva, A. F.; de Almeida, J. S.; Gazoto, A. L.; dos Santos, A. O.; Cardoso, L. P.; Meneses, E. A.; Graybill, D. L.; Mertes, K. M.
The structural, optical and electrical properties of InN polycrystalline films on glass substrate are investigated by means of X-ray photoelectron spectroscopy, Raman scattering measurements, X-ray diffraction analysis, optical spectroscopy, and electrical measurements as a function of the inverse of temperature. The absorption edge for the films is most likely due to an impurity band formed by the presence of defects in the material. Such an impurity band, located at 1.6 eV extends itself to about 1.8 eV above the Fermi level, and it is attributed to nitrogen vacancies present in the material. The Raman scattering data also reveal the incorporation of oxygen in the InN films, leading to the formation of the In2O3 amorphous phase during the process of sputtering. Additionally, the X-ray photoelectron spectroscopy of the valence band, which is highly desirable to the determination of the Fermi level, confirms the optical gap energy. Furthermore, the X-ray diffraction patterns of the thinner films present broader peaks, indicating high values for the strain between the film lattice and the glass substrate. Finally, first principles calculations are used to investigate the optical properties of InN and also to support the experimental findings.

Thin Solid Films, 520 [15], 4848-4852, 2012

[P105-12] "Suppression of Anderson localization of light in one-dimensional disordered photonic superlattices"

Reyes-Gomez, E.; Bruno-Alfonso, A.; Cavalcanti, S. B.; Oliveira, L. E.

The localization properties of electromagnetic modes in one-dimensional disordered photonic superlattices are theoretically studied. The multilayered system is considered to be composed of alternating stacks of two different random-thickness slabs, characterized by nondispersive and/or frequency-dependent electric permittivities and magnetic permeabilities. Results for the localization length are evaluated by using an analytical model for weakly disordered systems as well as its general definition through the transmissivity properties of the heterostructure. Good agreement between both results is observed only for small amplitudes of disorder. The critical frequencies at which the localization length diverges are correctly predicted in the whole frequency spectrum by the analytical model and confirmed via the corresponding numerical calculations. The lambda(2) dependence of the localization length, previously observed in disordered heterostructures made of material of positive refractive indexes, are confirmed in the present work. In addition, new lambda(4) and lambda(-4) dependencies of the localization length in positive-negative disordered photonic superlattices are obtained, under certain specific conditions, in the long and short wavelength limits, respectively. The asymptotic behavior of the localization length in these limits is essentially determined by the particular frequency dispersion that characterizes the metamaterial used in the left-handed layers. When the effects of absorption are considered, then a divergence of the localization length is still observed, under some conditions, in the short wavelength limit.

Physical Review B 85[19], 195110, 2012

[P106-12] "Technical and economic analysis of a power supply system based on ethanol reforming and PEMFC"

Lopes, D. G.; da Silva, E. P.; Pinto, C. S.; Neves, N. P.; Camargo, J. C.; Ferreira, P. F. P.; Furlan, A. L.; Lopes, D. G.

This work presents a technical and economic analysis of a power supply system based on a 5 kW Proton Exchange Membrane Fuel Cell (PEMFC) fed with hydrogen produced by the auto-thermal reforming of ethanol. The technical analysis is based on unpublished experimental data obtained from the prototype of an ethanol reformer developed by the Hydrogen Laboratory at Unicamp and by Hytron, which represents the state-of-the-art of this technology in Brazil. The results point out that the cost of the hydrogen produced by the ethanol reformer prototype is lower than the hydrogen prices in the Brazilian market, and that the cost of the electricity produced by that hydrogen in a PEMFC is lower than other alternative sources of energy, except when compared to the electricity available in grid-connected power system in Brazil.

Renewable Energy 45, 205-212, 2012

[P107-12] "Temperature dependence of coercive field of ZnFe2O4 nanoparticles"

Mendonca, E. C.; Jesus, C. B. R.; Folly, W. S. D.; Meneses, C. T.; Duque, J. G. S.; Coelho, A. A.

Structural and magnetic measurements on ZnFe2O4 nanoparticles obtained through co-precipitation chemical method are reported. The Rietveld analysis of X-ray patterns reveal that (i) our samples are single phase, and (ii) the average particle size increases with synthesis temperature. The zero-field-cooled (ZFC) and field-cooled (FC) magnetization measurements show that the average blocking temperature increases for increasing mean particle size. Besides, one can observe via magnetization measurements that our particle size distribution also increases as a function of synthesis temperature. Finally, we have observed that the coercive field does not decay with the square root of temperature following the Neel relaxation and the Bean--Livingston approaches. In order to fit our experimental data, we have used a generalized model that proposes a temperature dependence of blocking temperature due to the coexistence of blocked and unblocked particles. This proposed generalized model shows good agreement with our experimental results.

Journal of Applied Physics 111[5], 053917, 2012

[P108-12] "Theoretical investigation on the magnetocaloric effect in MnAs using a microscopic model to describe the magnetic and thermal hysteresis"

Alho, B. P.; de Oliveira, N. A.; de Sousa, V. S. R.; Gama, S.; Coelho, A. A.; Carvalho, A. M. G.; von Ranke, P. J.

We report the thermal and magnetic hysteresis diagram for mnAs that comes from a microscopic description of a magnetic system through a model Hamiltonian that takes into account the magnetoelastic interaction. The temperature and magnetic hysteresis intervals are governed by the magnetoelastic interaction parameter, which leads to the energy barrier between stable and metastable minima in the exact free energy, obtained from our microscopic model. Application of the model to the MnAs first-order magnetic material, which presents high hysteresis effect, leads to a good agreement with the experimental magnetic and magnetocaloric data.

Solid State Communications 152[11], 951-954, 2012

[P109-12] "Total hadronic cross section and the elastic slope: An almost model-independent connection"

Fagundes, D. A.; Menon, M. J.

An almost model-independent parametrization for the ratio of the total cross section to the elastic slope, as function of the center of mass energy, is introduced. The analytical result is based on the approximate relation of this quantity with the ratio R of the elastic to total cross section and empirical fits to the R data from proton proton scattering above 10 GeV, under the conditions of asymptotic unitarity and the black-disk limit. This parametrization may be useful in studies of extensive air showers and the determination of the proton-proton total cross section from proton-air production cross section in cosmic-ray experiments.

Nuclear Physics A 880, 1-11, 2012

[P110-12] "Ultrafast X-Ray Scattering of Xenon Nanoparticles: Imaging Transient States of Matter"

Bostedt, C.; Eremina, E.; Rupp, D.; Adolph, M.; Thomas, H.; Hoener, M.; de Castro, A. R. B.; Tiggesbaumker, J.; Meiwes-Broer, K. H.; Laarmann, T.; Wabnitz, H.; Plonjes, E.; Treusch, R.; Schneider, J. R.; Moller, T.

Femtosecond x-ray laser flashes with power densities of up to 10(14) W/cm(2) at 13.7 nm wavelength were scattered by single xenon clusters in the gas phase. Similar to light scattering from atmospheric microparticles, the x-ray diffraction patterns carry information about the optical constants of the objects. However, the high flux of the x-ray laser induces severe transient changes of the electronic configuration, resulting in a tenfold increase of absorption in the developing nanoplasma. The modification in opaqueness can be correlated to strong atomic charging of the particle leading to excitation of Xe4+. It is shown that single-shot single-particle scattering on femtosecond time scales yields insight into ultrafast processes in highly excited systems where conventional spectroscopy techniques are inherently blind.

Physical Review Letters 108[9], 093401, 2012

[P111-12] "Validation of diffuse correlation spectroscopic measurement of cerebral blood flow using phase-encoded velocity mapping magnetic resonance imaging"

Buckley, E. M.; Hance, D.; Pawlowski, T.; Lynch, J.; Wilson, F. B.; Mesquita, R. C.; Durduran, T.; Diaz, L. K.; Putt, M. E.; Licht, D. J.; Fogel, M. A.; Yodh, A. G.

Diffuse correlation spectroscopy (DCS) is a novel optical technique that appears to be an excellent tool for assessing cerebral blood flow in a continuous and non-invasive manner at the bedside. We present new clinical validation of the DCS methodology by demonstrating strong agreement between DCS indices of relative cerebral blood flow and indices based on phase-encoded velocity mapping magnetic resonance imaging (VENC MRI) of relative blood flow in the jugular veins and superior vena cava. Data were acquired from 46 children with single ventricle cardiac lesions during a hypercapnia intervention.Significant increases in cerebral blood flow, measured both by DCS and by VENC MRI, as well as significant increases in oxyhemoglobin concentration, and total hemoglobin concentration, were observed during hypercapnia. Comparison of blood flow changes measured by VENC MRI in the jugular veins and by DCS revealed a strong linear relationship, $R = 0.88$, $p < 0.001$, slope = 0.91 +/- 0.07. Similar correlations were observed between DCS and VENC MRI in the superior vena cava, $R = 0.77$, slope = 0.99 +/- 0.12, $p < 0.001$. The relationship between VENC MRI in the aorta and DCS, a negative control, was weakly correlated, $R = 0.46$, slope = 1.77 +/- 0.45, $p < 0.001$.

Journal of Biomedical Optics 17[3], 037007, 2012

Proceedings

[P112-12] "Combined nonlinear laser imaging (two-photon excitation fluorescence, second and third harmonic generation, and fluorescence lifetime imaging microscopies) in ovarian tumors"

Adur, J.; Pelegati, V. B.; de Thomaz, A. A.; Bottcher-Luiz, F.; Andrade, L. A. L. A.; Almeida, D. B.; Carvalho, H. F.; Cesar, C. L.

We applied Two-photon Excited Fluorescence (TPEF), Second/ Third Harmonic Generation (SHG and THG) and Fluorescence Lifetime Imaging (FLIM) Non Linear Optics (NLO) Laser-Scanning Microscopy within the same imaging platform to evaluate their use as a diagnostic tool in ovarian tumors. We assess of applicability of this multimodal approach to perform a pathological evaluation of serous and mucinous tumors in human samples. The combination of TPEF-SHG-THG imaging provided complementary information about the interface epithelium/ stromal, such as the transformation of epithelium surface (THG) and the overall fibrillar tissue architecture (SHG). The fact that H&E staining is the standard method used in clinical pathology and that the stored samples are usually fixed makes it important a re-evaluation of these samples with NLO microscopy to compare new results with a library of already existing samples. FLIM, however, depends on the chemical environment around the fluorophors that was completely changed after fixation; therefore it only makes sense in unstained samples. Our FLIM results in unstained samples demonstrate that it is possible to discriminate healthy epithelia from serous or mucinous epithelia. Qualitative and quantitative analysis of the different imaging modalities used showed that multimodal nonlinear microscopy has the potential to differentiate between cancerous and healthy ovarian tissue.

In: MULTIPHOTON MICROSCOPY IN THE BIOMEDICAL SCIENCES, 12., 2012, San Francisco. Proceedings... . Bellingham, Wa: Spie-int Soc Optical Engineering, 2012. v. 8226, 82261A.

[P113-12] "Influence of the growing parameters on the size distribution of PbTe nanoparticles produced by laser ablation under inert gas atmosphere"

Almeida, D. B.; Rodriguez, E.; Agouram, S.; Moreira, R. S.; Cesar, C. L.; Jimenez, E.; Barbosa, L. C.

We report the fabrication of PbTe quantum dots grown under inert gas (Ar and He) atmosphere by pulsed laser deposition using the second harmonic of a Q-Switched Quantel Nd:YAG laser. For characterization, samples were prepared onto a 40 angstrom carbon film deposited on a copper grid. The influence of background pressure, and number of laser pulses on the size distribution of the PbTe nanoparticles was investigated by transmission electron microscopy using a 200 kV TECNAI G2 F20 electron microscope with 0.27 nm point resolution. The size distribution was obtained by manually outlining the particles from several dozens of low-and high-resolution TEM images. Once digitized and saved in a proper format, the image was processed using the J-image software. Characterizations reveal an increase of the nanoparticle size both with the amount of material deposited (number of laser pulses) and the background pressure. Furthermore, measurements reveal a narrower nanoparticle size distribution by increasing the number of laser pulses or by decreasing the background pressure. HRTEM studies of the influence of different ambient gases on the structural properties of the PbTe nanoparticles are being conducted.

In: SYNTHESIS AND PHOTONICS OF NANOSCALE MATERIALS, 9., 2012, San Francisco, Ca. Proceedings... . Bellingham, Wa: Spie-int Soc Optical Engineering, 2012. v. 8245, 82450K.

[P114-12] "Multimodal optical setup for nonlinear and fluorescence lifetime imaging microscopies: improvement on a commercial confocal inverted microscope"

Pelegati, V. B.; Adur, J.; de Thomaz, A. A.; Almeida, D. B.; Baratti, M. O.; Carvalho, H. F.; Cesar, C. L.

In this work we proposed and built a multimodal optical setup that extends a commercially available confocal microscope (Olympus FV300) to include nonlinear optical (NLO) microscopy and fluorescence lifetime imaging microscopy (FLIM). The NLO microscopies included two-photon fluorescence (TPFE), Second Harmonic Generation (SHG) and Third Harmonic Generation (THG). The whole system, including FLIM, used only one laser source composed of an 80 MHz femtosecond laser. The commercial Ti:sapphire lasers can be tuned up to 690-1040 nm bringing the THG signal to the 350 nm region where most microscope optics do not work. However, the third harmonic is only generated at the sample, meaning that we only have to take care of the collection optics. To do that we used a remote photomultiplier to acquire the THG signal at the 310-350 nm wavelength window. After performing the tests to guarantee that we are observing actually SHG/THG signals we than used this system to acquire multimodal images of several biological samples, from epithelial cancer to vegetables. The ability to see the collagen network together with the cell nuclei proved to be important for cancer tissues diagnosis. Moreover, FLIM provides information about the cell metabolism, also very important for cancer cell processes.

In: IMAGING, MANIPULATION, AND ANALYSIS OF BIOMOLECULES, CELLS, AND TISSUES, 10. 2012. San Francisco, Ca. Proceedings... . Bellinghan, Wa. Spie-Int Soc Optical Engineering, 2012, v.8225, 82251I.

[P115-12] "Quantitative Second Harmonic Generation Imaging to Detect Osteogenesis Imperfecta in Human Skin Samples"

Adur, J.; Ferreira, A. E.; D'Souza-Li, L.; Pelegati, V. B.; de Thomaz, A. A.; Almeida, D. B.; Baratti, M. O.; Carvalho, H. F.; Cesar, C. L.

Osteogenesis Imperfecta (OI) is a genetic disorder that leads to bone fractures due to mutations in the Col1A1 or Col1A2 genes that affect the primary structure of the collagen I chain with the ultimate outcome in collagen I fibrils that are either reduced in quantity or abnormally organized in the whole body. A quick test screening of the patients would largely reduce the sample number to be studied by the time consuming molecular genetics techniques. For this reason an assessment of the human skin collagen structure by Second Harmonic Generation (SHG) can be used as a screening technique to speed up the correlation of genetics/phenotype/OI types understanding. In the present work we have used quantitative second harmonic generation (SHG) imaging microscopy to investigate the collagen matrix organization of the OI human skin samples comparing with normal control patients. By comparing fibril collagen distribution and spatial organization, we calculated the anisotropy and texture patterns of this structural protein. The analysis of the anisotropy was performed by means of the two-dimensional Discrete Fourier Transform and image pattern analysis with Gray-Level Co-occurrence Matrix (GLCM). From these results, we show that statistically different results are obtained for the normal and disease states of OI.

In: MULTIPHOTON MICROSCOPY IN THE BIOMEDICAL SCIENCES, 12., 2012, San Francisco. Proceedings... . Bellingham, Wa: Spie-int Soc Optical Engineering, 2012. v. 8226, 82263P.

Errata

"The Lateral Trigger Probability function for the Ultra-High Energy Cosmic Ray Showers detected by the Pierre Auger Observatory (vol 35, pg 266, 2011)"

Abreu, P.; Aglietta, M.; Ahn, E. J.; Albuquerque, I. F. M.; Allard, D.; Chinellato, J. A.; de Almeida, R. M.; de Mello Junior, W. J. M.; Dobrigkeit, C.; Escobar, C. O.; Kemp, E.; Muller, M. A.; Selmi-Dei, D. P.
Pierre Auger Collaboration

Astroparticle Physics 35[10], 681-684, 2012

Meeting Abstract

"EEG-fMRI Haemodynamic Responses of Patients with Non-Lesional Mesial Temporal Lobe Epilepsy (MTLE)"

Coan, A.; Beltramini, G.; Campos, B.; Covolan, R.; Cendes, F.

In: ANNUAL MEETING OF THE AMERICAN-ACADEMY-OF-NEUROLOGY (AAN), 64, 2012, New Orleans, La. Meeting. Philadelphia, Pa. Lippincott Williams & Wilkin, 2012. v. 78, supp. 1, P03113.

Defesas de Dissertações - Mestrado

[D001-12] "Impacto de Estações Irregulares sobre a Reconstrução de Eventos do Observatório Pierre Auger"

Aluno: Bruno Daniel
Orientador: Ernesto Kemp
Maio/2012

[D002-12] "O campo eletromagnético quantizado acoplado a um oscilador mecânico submetido a ruído"

Aluno: Maicon Zaniboni Siqueira
Orientador: Antonio Vidiella Barranco
Maio/2012

[D003-12] "Estratégias Computacionais para Escolha de Monômeros Funcionais para Síntese de Polímeros Molecularmente Impressos (MIP)"

Aluno: Francisco Alírio Almeida Gomes de Moura
Orientador: Douglas Soares Galvão
Maio/2012

[D004-12] "Oscilador Paramétrico Óptico Contínuo e Unicamente Ressonante no Infravermelho Próximo"

Aluno: Marina Trad Nery
Orientador: Flávio Caldas da Cruz
Junho/2012

Defesas de Teses - Doutorado

[T001-12] "Modelagem da distribuição de matéria em um Anel em presença de Shepherds, via equação de Fokker-Planck"

Aluno: Cesar Juan Alarcon Llacctarimay
Orientador: Maximiliano Ujevic Tonino
Maio/2012

[T002-12] "Fenomenologia de neutrinos atmosféricos com neutrinos de massa variável"

Aluno: Diego Rossi Gratieri
Orientador: Orlando Luis Goulart Peres
Maio/2012

[T003-12] "Estudo de Efeitos Quânticos na Termodinâmica da Matéria Condensada: transições de fase a temperatura finita"

Aluno: Bráulio Gabriel Alencar Brito
Orientador: Alex Antonelli
Junho/2012

Fonte: Portal IFGW / Pós-Graduação.
Disponível em: http://portal.ifi.unicamp.br/menu-pos-prod/menu-pos-prod-datadef

Abstracta

Instituto de Física
Diretor: Prof. Dr. Daniel Pereira
Universidade Estadual de Campinas - UNICAMP
Cidade Universitária Zeferino Vaz
13083-859 - Campinas - SP - Brasil
e-mail: secdir@ifi.unicamp.br
Fone: 0XX 19 3521-5300

Publicação

Biblioteca do Instituto de Física Gleb Wataghin
http://webbif.ifi.unicamp.br
Diretora Técnica: Sandra Maria Carlos Cartaxo

Elaboração
Maria Graciele Trevisan
graciele@ifi.unicamp.br

Projeto Gráfico
ÍgneaDesign

Impressão

Gráfica Central - Unicamp